Demonstration of Pattern Division Multiple Access With Message Passing Algorithm for Multi-Channel mmWave Uplinks via RoF Mobile Fronthaul

Shuyi Shen[®], You-Wei Chen[®], Qi Zhou[®], Jeff Finkelstein, and Gee-Kung Chang, Fellow, OSA

Abstract—Orthogonal multiple access (OMA) such as orthogonal frequency division multiple access (OFDMA) has been the predominant access technology adopted by the current generation of mobile communication. Representing an evolutionary step in radio access networks, non-orthogonal multiple access (NOMA) is considered to be a promising technology to meet the goals of increased capacity, enhanced flexibility, and reduced latency. Pattern division multiple access (PDMA) is a NOMA scheme using resource-element mapping as the multiple-access signature in the symbol level. This article introduces PDMA in a millimeter-wave (mmWave) radio access system with systematic experimental demonstration. One key advantage of PDMA is that it can facilitate advanced parallel interference cancellation (PIC) in the decoding process. A message passing algorithm (MPA) is developed and implemented in this article to enhance the decoding performance of PDMA. A novel PDMA system integrated with MPA is experimentally demonstrated in a multi-user mmWave radio access system that uses radio-over-fiber (RoF) mobile fronthaul, achieving reduced sensitivity penalty and improved modulation spectral efficiency compared to conventional power-domain NOMA (PD-NOMA) with successive interference cancellation (SIC). Experimental results show that PDMA is capable of supporting disparate channel conditions, adapting to various patterns, and providing improved system flexibility.

Index Terms—Message passing algorithm, non-orthogonal multiple access, pattern division multiplexing access.

I. INTRODUCTION

CCESS technologies in next-generation radio access networks (RANs) should be capable of adopting new spectrum resources and supporting different user-specific applications, as indicated in Fig. 1. One important technical approach of the fifth-generation New Radio (5G NR) is to utilize the abundant bandwidth in millimeter-wave (mmWave) bands. Considering both Friss propagation loss and atmospheric absorption loss in multi-user systems, mmWave links can exhibit dynamic

Manuscript received April 10, 2020; revised June 8, 2020; accepted June 26, 2020. Date of publication June 30, 2020; date of current version November 1, 2020. (Corresponding author: Shuyi Shen.)

Shuyi Shen, You-Wei Chen, Qi Zhou, and Gee-Kung Chang are with the School of Electrical and Computer Engineering, Georgia Institute of Technology, Atlanta, GA 30308 USA (e-mail: ssyzoe@gatech.edu; yu-wei.chen@ece.gatech.edu; qi.zhou@gatech.edu; geekung.chang@ece.gatech.edu).

Jeff Finkelstein is with Cox Communications, Atlanta, GA 30328 USA (e-mail: jeff.finkelstein@cox.com).

Color versions of one or more of the figures in this article are available online at https://ieeexplore.ieee.org.

Digital Object Identifier 10.1109/JLT.2020.3005905

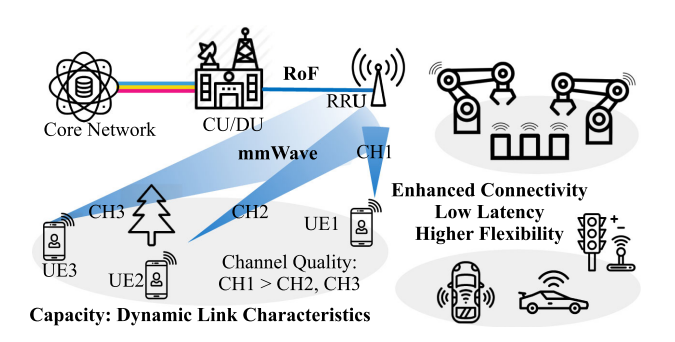


Fig. 1. Challenges for next-generation service-oriented RANs employing mmWave links with various channel qualities.

channel characteristics. To achieve high capacity under such complex link conditions can be a daunting task for conventional orthogonal multiple access (OMA) systems employed in current RANs and other wireless access networks [1]. Moreover, next-generation mobile data communication is anticipated to be service-oriented networks [2]. Use cases such as traffic safety, infrastructure protection, and industrial applications based on Internet of Things require low latency, an increased number of connected devices, and higher access flexibility. In response to these challenges, non-orthogonal multiple access (NOMA) has been investigated for 5G and next-generation RANs to exploit underutilized power resources and increase the number of access user equipment (UE) [3], [4]. Among various NOMA schemes, pattern division multiple access (PDMA) utilizes symbol-level UE-specific data signatures with sparse resource-element (RE) mapping [5], which is capable of providing improved flexibility with different pattern variants and supporting grant-free uplinks [6].

In a 5G mmWave small-cell structure as shown in Fig. 1, multiple users served by a remote radio unit (RRU) have to deal with different channel conditions. For example, there are users experiencing line-of-sight (LoS) links (UE₁, with channel 1, CH1), edge users which are far away from RRU experiencing low signal-to-noise ratio (SNR) and channel gain due to high path loss (UE₂ with CH2), or users suffering severe channel degradation (UE₃ with CH3) due to LoS blockage or antenna misalignment of the mmWave links. When managing multiple UEs with disparate reception qualities, RRUs employing conventional orthogonal frequency-division multiple access (OFDMA) have to trade off spectral efficiency to serve low-SNR

0733-8724 © 2020 IEEE. Personal use is permitted, but republication/redistribution requires IEEE permission. See https://www.ieee.org/publications/rights/index.html for more information.

users with low-order QAM modulation [1]. Recognizing these system limitations, NOMA is proposed to enhance capacity by exploiting power-domain multiplexing for multi-user access. As a NOMA scheme based on OFDM, PDMA assigns spreading patterns to differentiate users sharing the same time-frequency resource block. With the pattern used as the third dimension for resource sharing, PDMA can provide better access opportunities and flexibility in resource allocation through customized RE mapping, power scaling and/or phase shifting of the pattern matrix. In addition, PDMA can improve latency performance in the two ways; (i) for the contention-based mechanism, the resource pool is expanded, which reduces the probability of collisions; and (ii) for grant-free uplinks, the expanded resource pool can provide more pre-assigned user-specific signatures. In addition, advanced decoding techniques supported by PDMA allow reduced power level of grant-free uplinks, which can reduce the interference on existing underlaying normal data.

One important advantage of PDMA is that it facilitates parallel interference cancellation (PIC) in the receiver digital signal processing (DSP). As a comparison, successive interference cancellation (SIC) is used in conventional NOMA. SIC is susceptible to error propagation which makes the decoding of the received signal highly dependent on the error rate of precedent users[7]. As one of the PIC schemes, message passing algorithms (MPA) can be applied to enhance decoding accuracy for PDMA coded with sparse patterns. This is because MPA can approximate maximum *a posteriori* detection through algorithms based on factor graph, an equivalent representation of a pattern matrix. Owing to significantly enhanced decoding capability, PDMA with MPA will induce less interference on REs shared by multiple UEs, which can further support low-latency services with grant-free uplinks.

In this paper, PDMA integrated with MPA is developed for multi-user uplinks in a mmWave radio access system using radio-over-fiber (RoF) mobile fronthaul. The paper is an extension of our recent work published in [8], with expanded research results validated by theoretical analysis and comprehensive experimental demonstration. The remainder of this paper is organized as follows. Section II introduces the basics of PDMA with examples illustrating the implementation process and factors affecting PDMA performance. The principles of MPA and our modification thereof are also presented. Section III summarizes the experimental setup and system design. Experimental demonstration and results are analyzed and discussed in Section IV, which covers several aspects of PDMA performance including the comparison of MPA and SIC, the flexibility provided by PDMA, the support for grant-free uplinks, and normal data transmission under channel degradation. Finally, the paper is concluded in Section V.

II. FUNDAMENTALS OF PDMA AND MPA

PDMA is an OFDM-based NOMA scheme operating on the symbol level, combined with sparse RE mapping. For K users sharing N subcarriers ($K \ge N$), the key design element in PDMA is the pattern matrix. The pattern matrix defines how different users share the same resource block non-orthogonally.

Three main functions of the pattern matrix are: 1) it provides the mathematical description and guidance for RE allocation; 2) the matrix can be tuned and optimized for interference control; 3) the symbol diversity in the matrix allows PIC. In this section, we will first introduce the basics of PDMA and its notations followed by the principles of MPA.

A. Basics of PDMA

The pattern matrix is an binary matrix (containing only 1 and 0) that is defined as: $\mathbf{P}^{[N,K]} = [\mathbf{p}_1, \mathbf{p}_2, \dots, \mathbf{p}_K]$, where \mathbf{p}_k is an $N \times 1$ pattern vector that can be assigned to different streams/users[9]. The diversity order D_k of a pattern vector is equal to the number of '1's in the vector. For K streams sharing the same resource block, there are K QAM symbols in the original symbol vector $\mathbf{x} = [x_1, x_2, \dots, x_K]^T$. The transmitted symbol vector \mathbf{s}_k of stream k is obtained by spreading x_k according to pattern vector \mathbf{p}_k : $\mathbf{s}_k = \mathbf{p}_m x_k$, where \mathbf{s}_k is an $N \times 1$ vector. The amplitude and phase of each stream can be tuned to achieve the desired constellation for better interference control [5]. The scaling matrix is introduced for the scaling process: $\mathbf{A}^{[N,K]} = \mathbf{i}\mathbf{a}$, where $\mathbf{a} = [a_1, a_2, \dots a_K]$ is a $1 \times K$ vector with $a_k = \alpha_k e^{j\beta_k}$ comprising the amplitude (α_k) and phase (β_k) , and $\mathbf{i} = [1, 1, \dots, 1]^T$ is an $N \times 1$ vector. In PDMA, one user can be assigned one or multiple streams. Therefore, the transmitted signal vector for each user is $t_i = \sum_{k \in UE_i} a_k s_k$, where t_i is an $N \times 1$ vector, and will be passed to next-stage OFDM processing. At the receiver, the corresponding channel response is: $\mathbf{H}^{[N,K]} = [\mathbf{h}_1, \mathbf{h}_2, \dots, \mathbf{h}_K]$, where \mathbf{h}_k is an $N \times 1$ vector, with many 0's in accordance to \mathbf{p}_k . As a result, the received signal vector in the frequency domain after preliminary OFDM processing will be: $\mathbf{r} = (\mathbf{H} \odot \mathbf{A} \odot \mathbf{P})\mathbf{x} + \boldsymbol{\nu}$. Here \odot is the element-wise product and ν is the additive white Gaussian noise (AWGN).

Pattern vectors can be assigned to users in different ways to meet the requirements of various applications. It is worth noting that the received constellation can be influenced by the stream amplitude/phase tuning at the transmitter (Tx), modulation orders, and channel gain. In our experiments, streams are grouped and assigned to two users, given two sets of transmitters operating at mmWave frequency. Two examples are given in Fig. 2 to illustrate stream-user assignment, stream tuning (a), and QAM order assignment where bpS stands for bits per symbol, e.g. bpS = 4 corresponds to 16QAM.

Shown in Fig. 2(a) is case A where four subcarriers are shared by six streams assigned to two users, with $UE_1 = \{1,4,5\}$ and $UE_2 = \{2,3,6\}$. Case A is an example of grant-free uplinks supported by PDMA. In the basic upstream scheduling process in mobile communications, users first request then wait for the grant distributed by the scheduler before payload data transmission [10]. In grant-based random access, resource blocks are selected and granted for a user at each time slot. In contrast, a user under grant-free access scheme is pre-assigned a unique user signature used for all time slots [6]. PDMA can skip the request-grant process by pre-assigning user-specific patterns for grant-free uplinks, therefore reducing latency. To achieve effective grant-free uplinks, methods such as joint user activity and data

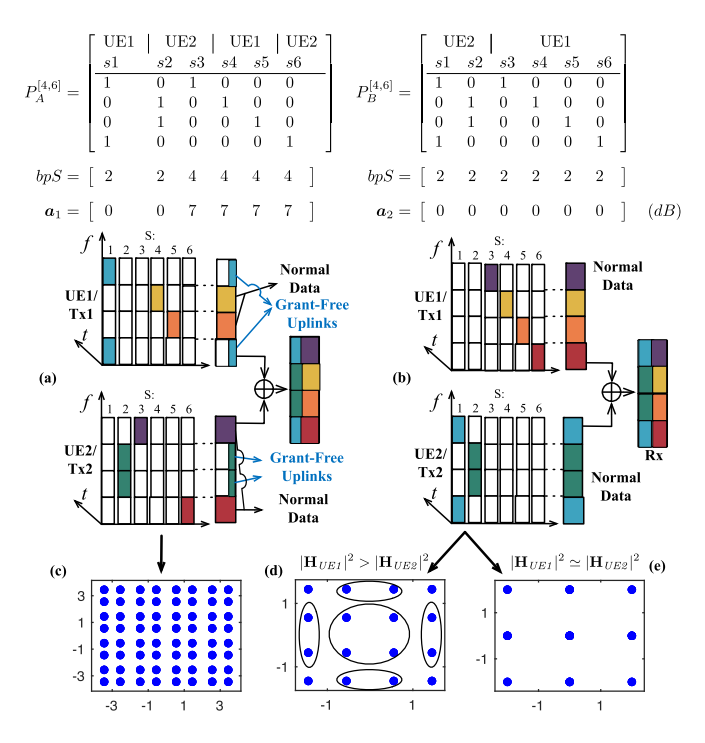


Fig. 2. (a) Case A for grant-free uplinks; (b) Case B for normal data transmission. Received constellation: (c) Case A; (d) Case B when UE_1 channel gain is larger than UE_2 ; (e) Case B when both users experience similar channels (constellation ambiguity).

detection should be employed and have been discussed in [11], [12]. For OMA, it is challenging to provide a sufficient number of orthogonal user signatures for pre-assigning, especially with the requirement of massive connectivity. Plus, time-frequency grids may be under-utilized in this case. While in PDMA, a pattern vector can be pre-assigned and reserved for a user as a third-dimension user signature on top of time and frequency dimensions. In this case, the cost of grant-free access is the interference among users sharing the same RE. Using PDMA integrated with MPA allows grant-free streams to co-exist with normal data streams, with a proper pattern design. Owing to the diversity of the symbol as well as the decoding capability of MPA, the required power level of the grant-free streams can be reduced to lower the interference on other streams sharing the same RE, without significantly sacrificing the performance.

The resource allocation process is visualized in Fig. 2(a). The pattern of stream 1 (s1) is pre-assigned to UE₁ for grant-free uplinks, whereas s4 and s5 are allocated for normal data transmission. s1 has a much lower power level but higher diversity ($D_{s1}=2$) compared to s4 and s5 ($D_{s4,s5}=1$), resulting in reduced interference on the other user that may be using the same REs. Given the corresponding stream amplitude tuning vector a_1 , QAM order assignment, and similar channel conditions experienced by both users, the received constellation is depicted in Fig. 2(c).

In the case of normal data transmission, case B, the same pattern matrix is used but with different stream-user assignment, modulation orders, and stream amplitude tuning, as shown in Fig. 2(b). Both users utilize all four subcarriers. UE₂ is assigned

two streams with higher diversity to cope with possible channel degradation. The received constellation under two different channel conditions are shown in Fig. 2(d) and (e). When the channel gain of UE₁ is significantly higher than UE₂ (7 dB in Fig. 2(d)), the received constellation is similar to 16QAM due to the superposition of signals from two UEs. However, the received constellation will degenerate to that shown in Fig. 2(e) when the channel gain of both users are on the same level, in which case one constellation point can represent multiple combinations of QAM symbols. In this case, constellation ambiguity occurs and should be considered in the decoding process.

B. Message Passing Algorithm

Patterns used in PDMA bring diversity of the original symbols. In our demonstration, MPA is implemented in the receiver DSP to fully utilize this diversity. In MPA, the decoding process is based on information passing across the factor graph, which is determined by the pattern matrix. After several iterations of information exchanges and upon reaching convergence, MPA decodes all Tx symbols x simultaneously, in contrast to SIC where users are decoded successively.

At the receiver, the received symbol r_n at RE n is:

$$r_n = \sum_{k=1}^{K} h_{n,k} a_k p_{n,k} x_k + \nu_n \triangleq \sum_{k=1}^{K} f_{n,k} x_k + \nu_n$$
 (1)

Here $f_{n,k}$ is the effective signature element that includes channel distortion $(h_{n,k})$, stream amplitude/phase tuning (a_k) , and the element of PDMA matrix $(p_{n,k})$. Let ξ_n and ζ_k be the set of 1's positions in the n_{th} row and the k_{th} column of the pattern matrix, respectively. Then eq. (1) becomes:

$$r_n = \sum_{k \in \xi_n} f_{n,k} x_k + \nu_n = \mathbf{f}^{[n]T} \mathbf{x}^{[n]} + \nu_n$$
 (2)

where $\mathbf{x}^{[n]}$ denotes the vector containing the symbols from streams participating in the n_{th} row and $\mathbf{f}^{[n]}$ denotes the corresponding fraction of effective signature values.

The maximum *a posteriori* estimation for x is:

$$\hat{\mathbf{x}} = \arg \max_{\mathbf{x} \in \mathbb{X}^K} p(\mathbf{x}|\mathbf{r}) \tag{3}$$

From Bayes rule, we have:

$$p(\mathbf{x}|\mathbf{r}) = \frac{p(\mathbf{r}|\mathbf{x})P(\mathbf{x})}{P(\mathbf{r})} \propto p(\mathbf{r}|\mathbf{x})P(\mathbf{x})$$
(4)

in which $P(\mathbf{x}) = \prod_{k=1}^K p(x_k)$ is the joint *a priori* probability of the original symbol vector as the symbols are independent identically distributed (i.i.d.) and $P(\mathbf{r}) = \sum_{\mathbf{x} \in \mathbb{X}^K} p(\mathbf{r}|\mathbf{x})P(\mathbf{x})$ is the probability of the received symbol vector. Furthermore, with the assumption that noise is i.i.d. and uncorrelated with the transmitted symbols, we have:

$$p(\mathbf{r}|\mathbf{x}) = \prod_{n=1}^{N} p(r_n|\mathbf{x}) = \prod_{n=1}^{N} p(r_n|\mathbf{x}^{[n]})$$
 (5)

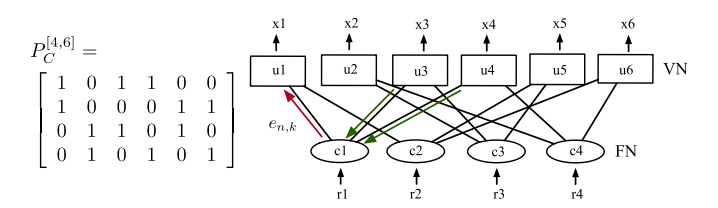


Fig. 3. An example of a factor graph with corresponding pattern matrix.

Assume that the channel estimation is available at the receiver, under AWGN channel the probability of r_n given $\mathbf{x}^{[n]}$ is:

$$p\left(r_n|\mathbf{x}^{[n]}\right) = \frac{1}{\sqrt{2\pi}\sigma} \exp\left(-\frac{1}{2\sigma^2} \left\|r_n - \mathbf{f}^{[n]T}\mathbf{x}^{[n]}\right\|^2\right)$$
(6)

Furthermore, combining eq. (3), (4), and (5), the estimation for x_k can be obtained by maximizing the marginal probability:

$$\hat{x}_{k} = \arg \max_{q \in \mathbb{X}_{k}} \sum_{\substack{\mathbf{x} \in \mathbb{X}^{K} \\ x_{k} = q}} p(\mathbf{x}|\mathbf{r})$$

$$= \arg \max_{q \in \mathbb{X}_{k}} \sum_{\substack{\mathbf{x} \in \mathbb{X}^{K} \\ x_{k} = q}} P(\mathbf{x}) \prod_{n \in \zeta_{k}} p\left(r_{n}|\mathbf{x}^{[n]}\right)$$
(7)

in which q is a symbol in constellation alphabet X_k .

From eq. (3) to (7), the marginal probability x_k is calculated instead of joint probability. In MPA, the decoding complexity is further reduced by approximating the marginal probability calculation iteratively over the underlying bipartite factor graph [13]. Fig. 3 shows an example of a factor graph and the corresponding pattern matrix P_C . From the pattern matrix to the factor graph, each column (x_k) corresponds to a variable node (VN, u_k) and each row (r_n) corresponds to a function node (FN, c_n). Each edge $e_{n,k}$ in the factor graph means that the corresponding $p_{n,k}=1$. In MPA process, messages containing the inference of x_k are passed along the edges and updated in the FNs and VNs, using respective update functions. The MPA used in our demonstration is at the symbol level. When there are cycles in the factor graph, the iterative calculation will become an approximation of eq. (7).

Provided that high-order QAM modulations are used, the message being exchanged along $e_{n,k}$ is a set with size $|\mathbb{X}_k|$, comprising the (inference) probability of symbols in $|\mathbb{X}_k|$. In each round of update, a node will collect messages from all of its connected nodes. It is worth noting that the message received by a node should be extrinsic, meaning that the message received from one edge cannot be used later to update the message to be transmitted onto that edge [13]. As shown in Fig. 3, the message conveyed by the red arrow only contains the messages from the green arrows, despite the fact that c_1 has the access to the messages from all three nodes (u_1, u_3, u_4) .

Let $\ell_{c_n \to u_k}$ be the message set sent along $e_{n,k}$ from c_n to u_k , then the message should only have extrinsic information:

$$\ell_{c_n \to u_k} = \left\{ p(x_k = q | r_n, \mathbf{x}^{[n]} \backslash x_k), \forall q \in \mathbb{X}_k \right\}$$
 (8)

Based on eq. (7), the message should include the product of the messages received from edges $e_{n,l}, \forall l \in \xi_n \backslash k$, as well as the observation at c_n using local function $p(r_n|\mathbf{x}^{[n]})$. In our

demonstration, the message element takes the maximum value in eq. (7) instead of summation for achieving better convergence efficiency. Therefore, the message element is:

$$\ell_{c_n \to u_k}(x_k = q) \triangleq p(x_k = q | r_n, \mathbf{x}^{[n]} \setminus x_k)$$

$$= \max_{\substack{x_k = q \\ \mathbf{x}^{[n]} \in \mathbb{X}^{d_{c,n}}}} \left(\prod_{l \in \xi_n \setminus k} \ell_{c_n \leftarrow u_l}(x_l) \right) \cdot p\left(r_n | \mathbf{x}^{[n]}\right)$$

$$p\left(r_n | \mathbf{x}^{[n]}\right) = \frac{1}{\sqrt{2\pi}\sigma} \exp\left(-\frac{1}{2\sigma^2} \left\| r_n - \mathbf{f}^{[n]T} \mathbf{x}^{[n]} \right\|^2\right)$$
(9)

in which $d_{c,n}$ is the number of streams involved in r_n . Similarly, the message set sent from u_k to c_n will be the product of the messages received from edges $e_{m,k}, \forall m \in \zeta_k \backslash n$:

$$\ell_{c_n \leftarrow u_k} = \left\{ \lambda_k \prod_{m \in \zeta_k \setminus n} \ell_{c_m \to u_k}(x_k = q), \forall q \in \mathbb{X}_k \right\}$$
 (10)

in which λ_k is chosen such that the sum of probabilities for all q is 1. After the MPA converges or the number of iterations reaches a pre-set maximum, the probability of $x_k = q$ is:

$$p(x_k = q) = \lambda_k' \prod_{n \in \zeta_k} \ell_{c_n \to u_k}(x_k = q)$$
 (11)

Finally, we have the estimation of x_k as provided by the MPA:

$$\hat{x}_k = \arg\max_{q \in \mathbb{X}_k} p(x_k = q) \tag{12}$$

Let d_C be the average number of superimposed streams in one RB, $|\mathbb{X}|$ be the average alphabet size, and T_i be the number of iterations processed. Note that FN updates (eq. (8)) take the primary computation complexity, the complexity of MPA (the number of multiplication operations) is hence [5]:

$$O(T_i N d_C |\mathbb{X}|^{d_C}) \tag{13}$$

As a comparison, the complexity of SIC (the number of addition operation) is:

$$O(N|\mathbb{X}|^{d_C}) \tag{14}$$

MPA can achieve improved decoding efficiency with higher computational complexity. The complexity of MPA can be reduced by restricting the average number of superimposed streams at the same RB (d_C) or restricting the maximum number of iterations.

III. EXPERIMENTAL SETUP

The experimental setup is depicted in Fig. 4. Two UEs access the RRU via mmWave uplinks and analog RoF mobile fronthaul. K_i PDMA streams in $UE_i = \{s_{i,1}, s_{i,2}, \ldots, s_{i,K_i}\}$ are assigned to UE_i. In the Tx-side DSP for each UE_i, K_i streams of bits are modulated to QAM symbols. Symbols within each stream use the same QAM order. QAM symbols are spread, scaled, and mapped to REs in accordance with the pattern matrix. Streams belonging to UE_i are summed and go through conventional OFDM DSP. The subcarrier spacing is $2^7 \times 15 \text{ kHz} = 1.92 \text{ MHz}$ compliant with 5G standards. The FFT size is 2048, 420 out of which carry the payload. Subcarriers

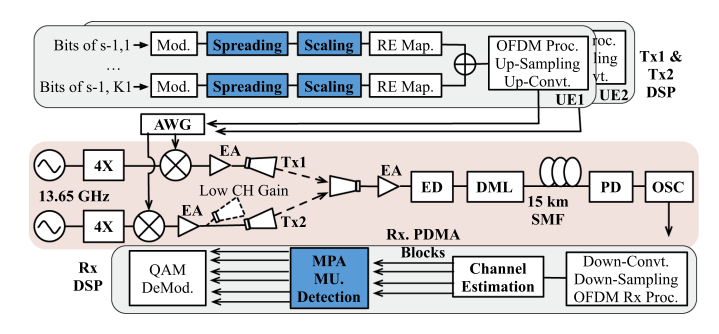


Fig. 4. Experimental setup.

are partitioned and grouped in order to apply the pattern matrix. The intermediate frequency is 510 MHz and the effective signal bandwidth is 806.4 MHz.

The digital OFDM signal is converted to analog waveform via an arbitrary waveform generator (AWG, sampling rate 15.73 GSa/s). At each Tx, 54.59 GHz carrier frequency is generated by a 13.65 GHz radio-frequency (RF) source followed by a quadrupler. Each AWG output signal is upconverted to the RF carrier by a mixer. The synthesized mmWave signal is then each amplified by an electrical amplifier (EA), transmitted by a horn antenna with 25 dBi. The wireless transmission distance is 1.5 m. At the receiver (Rx), another horn antenna captures both signals from the two UEs. The received signal is down-converted by an envelope detector (ED, 1 GHz). The baseband electrical signal is then converted to the optical domain through a directly modulated laser diode (DML, 2.5 GHz). After transmission over 15 km standard single-mode fiber (SMF), the signal is captured by a photodetector (PD, 2.5 GHz) and input into an oscilloscope (OSC, 5 GSa/s) followed by offline DSP. At the Rx, the received signal goes through preliminary OFDM demodulation and channel estimation which is essential for MPA detection. Received symbols are re-organized into resource blocks in accordance with the pattern matrix. MPA is applied to every received block to recover K_i streams of QAM symbols which are then decoded to K_i bit streams for bit-error-rate (BER) calculation. To investigate how PDMA can be tailored to support different application scenarios, the channel gain of Tx2 is varied during the experiments. In some experimental cases, UE2 will experience low channel gain, controlled by the AWG output power of Tx2.

IV. EXPERIMENTAL RESULTS

Four categories of experiments were carried out to verify the performance of PDMA with MPA: i) Comparison of MPA and SIC; ii) the flexibility of PDMA with different pattern matrices and channel conditions; iii) PDMA for grant-free uplinks (case A); iv) PDMA for normal data transmission under channel degradation (case B). In the experiments, BER versus received optical power (ROP) at the PD was measured and analyzed.

A. Comparison of MPA and SIC

The PDMA parameters used in the experiment are the same as those in case A illustrated in Section II-A, Fig. 2(a), in which

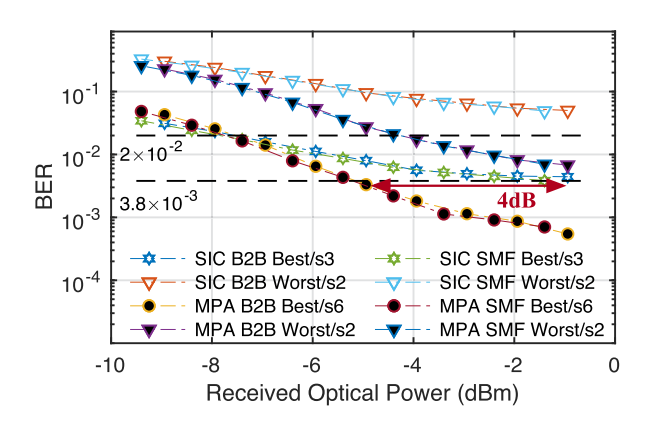


Fig. 5. Comparison of MPA and SIC.

 $UE_1=\{1,4,5\}$ and $UE_2=\{2,3,6\}$. The channel gain for UE₁ and UE₂ is on the same level, i.e. $|\mathbf{H}_{UE1}|^2\simeq |\mathbf{H}_{UE2}|^2$. In the experiment, SIC is evaluated and compared to MPA. In SIC, the stream with higher power level will be decoded first. For example, for the received symbol r_1 , \hat{x}_3 will be decoded first and then subtracted for the decoding of \hat{x}_1 . Fig. 5 selects streams with the best (from streams with high power level) and worst (from streams with low power level) BER performance, both in back-to-back (B2B) and after transmission over 15 km SMF. Experimental results show that MPA detection can achieve an approximate 4 dB Rx sensitivity improvement at 7% hard-decision forward error correction (HD-FEC) threshold compared to SIC, providing 1.9 GbpS for each UE.

At 20% soft-decision FEC (SD-FEC) threshold, the improvement of MPA for steams with the best BER performance is limited. In this region, the system is mainly restricted by bad SNR. MPA achieves enhanced decoding performance owing to information passed and verified over the factor graph, the accuracy of which is essentially built on the error rate of each node. At around the 20% SD-FEC limit, the error rate of each node is already high, resulting in the degraded performance of MPA.

The performance of MPA and SIC under constellation ambiguity is also evaluated. The pattern matrix and user-stream assignment is the same as those used in Fig. 5. The modulation of all streams is QPSK, i.e. $bpS = [2\ 2\ 2\ 2\ 2]$, the stream amplitude tuning is $a = [0\ 0\ 0\ 0\ 0]$ dB, and the channel condition is $|\mathbf{H}_{UE1}|^2 \simeq |\mathbf{H}_{UE2}|^2$. With such parameter setting, the constellation ambiguity will occur as indicated in Fig. 2(e). It can be seen from Fig. 6 that SIC is not able to differentiate ambiguous symbols with BER value all beyond 7% HD-FEC threshold threshold, whereas MPA can achieve acceptable BER performance with high ROP.

B. Flexibility Provided by PDMA

PDMA can be easily adapted to meet requirements of different bit rate, interference level, and reliability, owing to the tunability of the pattern matrix and stream amplitude/phase tuning. In this category of experiments, we first investigate different pattern matrices. Fig. 7 shows two scenarios supported by different pattern matrices: P_A (Section II-A, Fig. 2(a)) and P_C

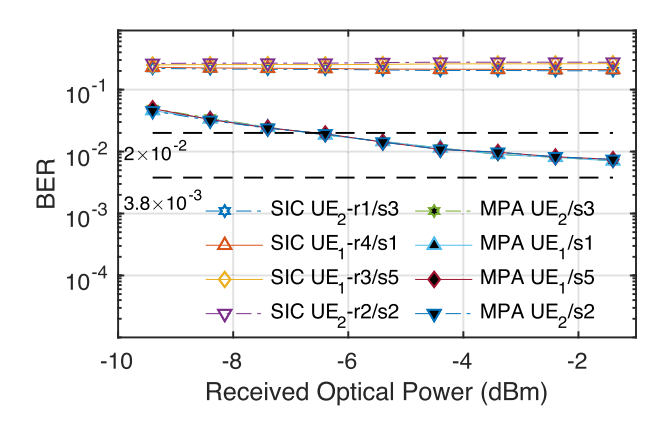


Fig. 6. Comparison of the BER for MPA and SIC when constellation ambiguity occurs. In the legend, ' $r_1/s3$ ' corresponds to the measured BER in the presence of s3 in the received symbol r_1 during SIC detection.

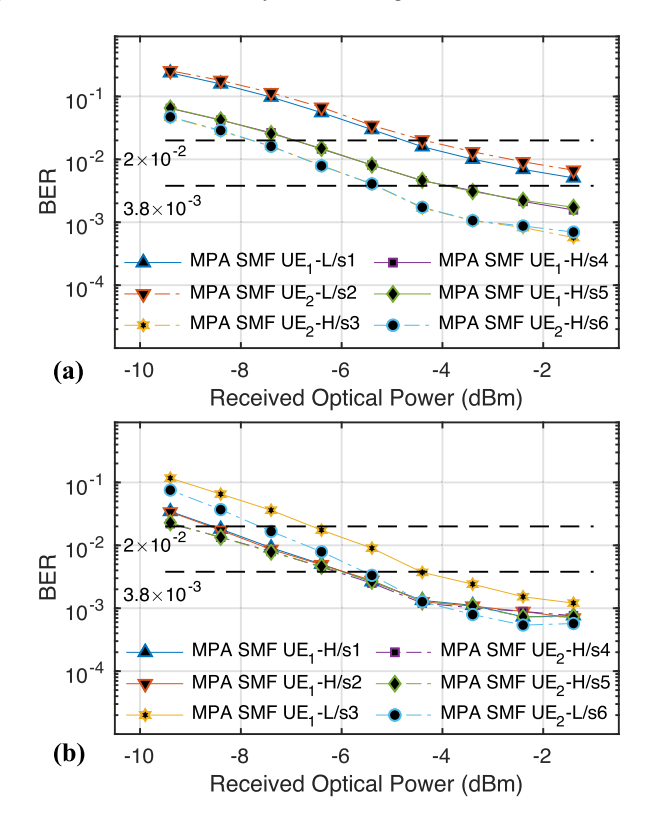


Fig. 7. Comparison of two pattern matrices: (a) P_A and (b) P_C . In the legend, 'H'/'L' corresponds to the streams with high(H)/low(L) amplitudes.

(Section II-B, Fig. 3). The user-stream allocation, stream amplitudes, modulation order, and channel condition of Fig. 7(a) are the same as case A. Whereas the parameters used in Fig. 7(b) are: $UE_1 = \{1, 2, 3\}$ and $UE_2 = \{4, 5, 6\}$, $\boldsymbol{a} = [770770]$ dB, bpS = [2222], and $|\mathbf{H}_{UE1}|^2 \simeq |\mathbf{H}_{UE2}|^2$. P_C has the same matrix size as P_A (4 × 6), but has higher average diversity. The symbols of every stream in P_C is spread twice, resulting in better decoding reliability at the cost of reduced data rates of s3 to s6. Consequently, P_C has better overall BER performance in comparison to P_A as shown in Fig. 7(b) and (a).

We also investigate the capability of PDMA handling varied channel qualities. In the experiment, we use the same PDMA setting as case B in Section II-A, Fig. 2(b), but with varied user

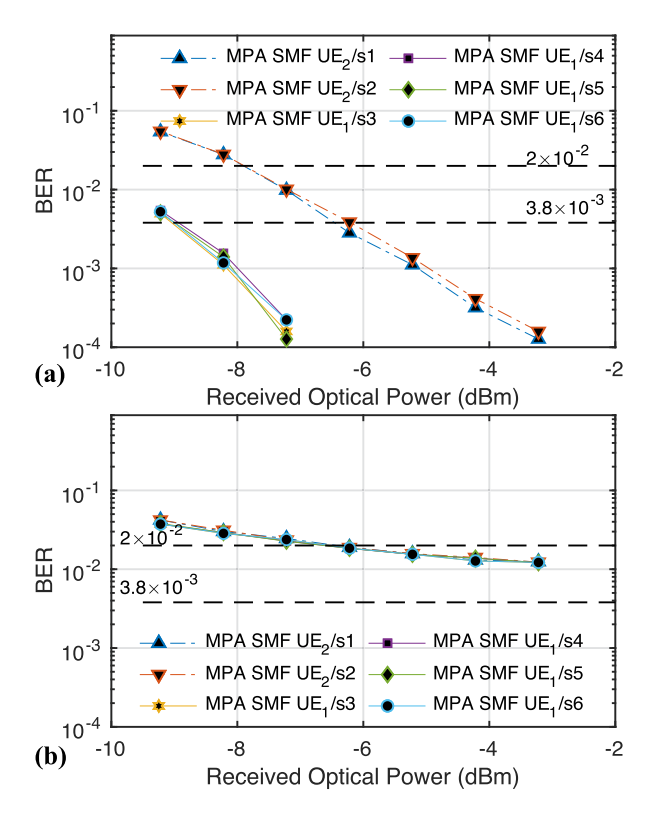


Fig. 8. BER vs. ROP performance when UE₁ and UE₂ have the same Tx PDMA setting, with varied channels: (a) $|\mathbf{H}_{UE1}|^2 \simeq |\mathbf{H}_{UE2}|^2 + 7 \text{ dB}$; (b) $|\mathbf{H}_{UE1}|^2 \simeq |\mathbf{H}_{UE2}|^2$.

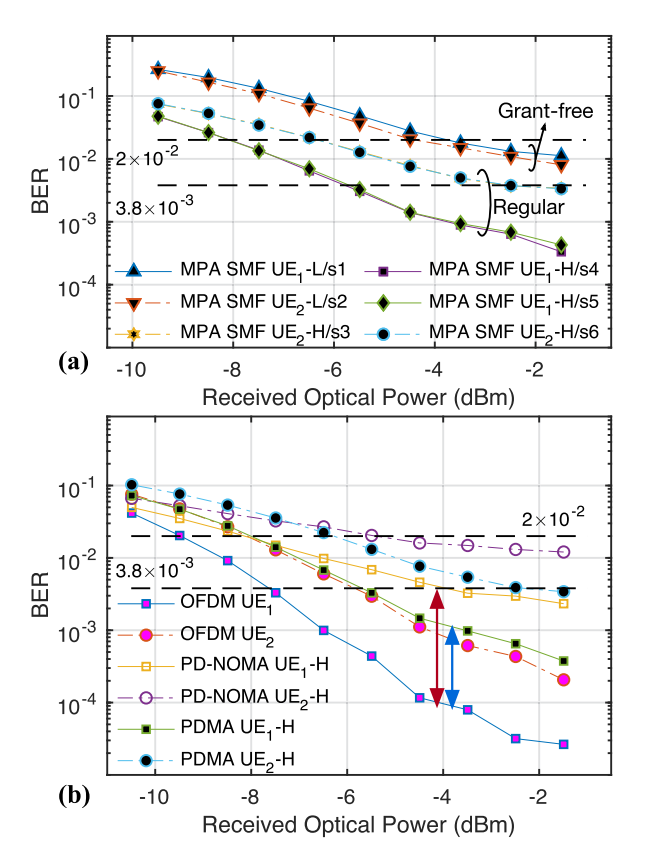


Fig. 9. Experimental results of case A: (a) BER vs. ROP; (b) Penalty of PDMA and PD-NOMA compared to interference-free OFDM.

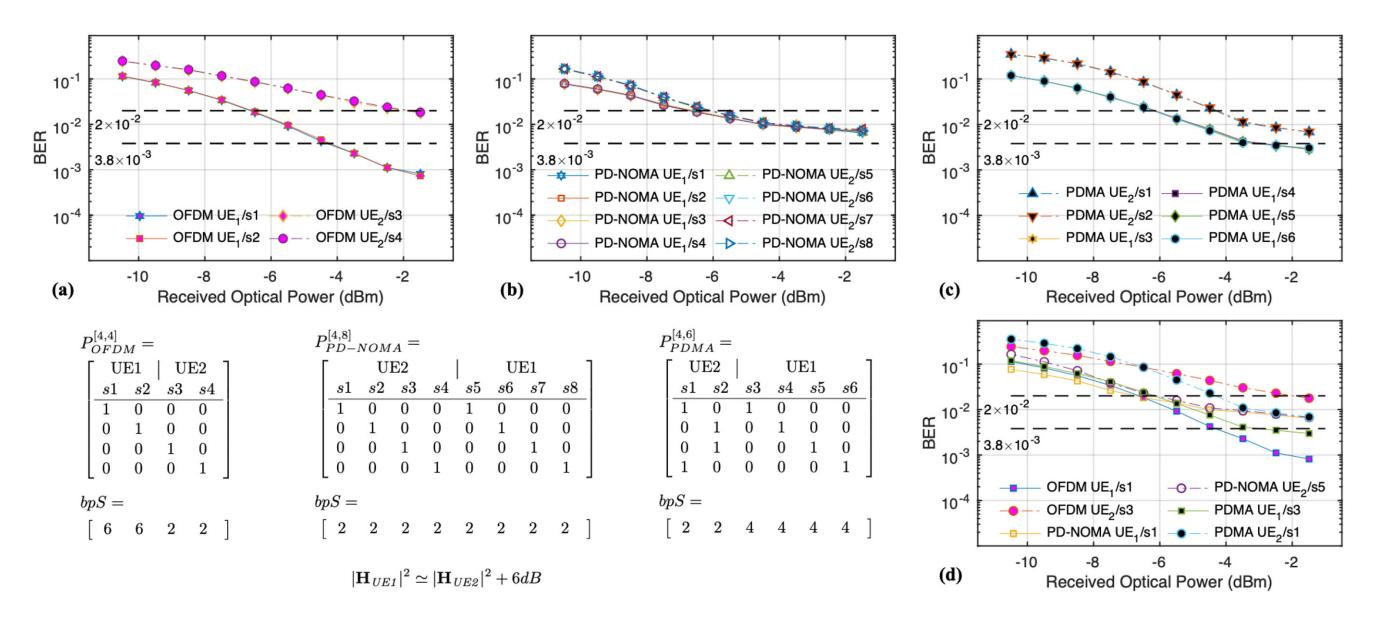


Fig. 10. BER of case B when $|\mathbf{H}_{UE1}|^2 > |\mathbf{H}_{UE2}|^2$, supported by (a) OFDM; (b) PD-NOMA-SIC; (c) PDMA-MPA. (d) Summary of (a), (b), and (c).

channel qualities. In Fig. 8(a), $|\mathbf{H}_{UE1}|^2 \simeq |\mathbf{H}_{UE2}|^2 + 7 \, \mathrm{dB}$; in Fig. 8(b), $|\mathbf{H}_{UE1}|^2 \simeq |\mathbf{H}_{UE2}|^2$. From Fig. 8(a) to (b), BER degradation can be observed due to the increased interference from UE₂ to UE₁ which causes it to approach constellation ambiguity. Owing to MPA, the UEs can maintain BER below threshold given channel gain varying over 7 dB, without changing the PDMA Tx-side setting.

From the experimental results shown in Fig. 5–8, the BER performance of PDMA can be affected by stream amplitude/phase tuning and pattern matrix design, which provides more configuration flexibility, in addition to the improved system turbulence immunity provided by MPA.

Similar to other NOMA schemes, PDMA stacks multiple symbols in one RE. The decodability of the system is dependent on the signal to noise and interference ratio which is determined by system SNR and number of users. Provided with higher SNR, one RE can be shared by more users. On the other hand, the system can support more users if lower modulation order is applied. For example, the system SNR can support the co-transmission of a QPSK symbol and a 16QAM symbol from two users at one RE (Fig. 5), as well as the co-transmission of three QPSK streams (Fig. 7(b)) using pattern matrix P_C . In our demonstration, a two-user scenario is implemented given two sets of Tx available at mmWave frequencies, in which each user is assigned multiple streams. In applications without the device limitation, one stream can correspond to one user, which can support increased number of users. The total number of users is dependent on achievable SNR, modulation order used, and the design of PDMA pattern matrix.

C. PDMA for Grant-Free Uplinks

As illustrated in case A, $UE_1 = \{1, 4, 5\}$, among which s1 with lower amplitude level is pre-assigned for grant-free uplinks and stacked onto normal data of s3 and s6 that are sharing the same REs. Fig. 9(a) verifies that both grant-free

uplinks and normal data transmission can be supported by PDMA with BER of all six streams below the FEC threshold when ROP > -4 dBm. To investigate how interference from grant-free uplinks affects normal data transmission, the BER of PDMA-MPA, PD-NOMA-SIC, and interference-free OFDM were evaluated. As shown in Fig. 9(b), the BER of the streams with high power for normal data transmission are compared with interference-free OFDM streams. It can be seen that at ROP = -4 dBm, for UE₁ the BER of OFDM is around 10^{-4} , the BER of PDMA stream degrades to approximately 10^{-3} , whereas the BER of PD-NOMA-SIC drops to about 3.8×10^{-3} . Owing to the improved decoding accuracy of MPA, the penalty from the grant-free uplinks supported by PDMA is mitigated compared to that of PD-NOMA-SIC.

D. PDMA for Normal Data Transmission Under Channel Degradation

As mentioned in the introduction, OMA such as OFDMA has to trade off spectral efficiency when part of the users are experiencing low-SNR channels. In this experiment, the performance of PDMA, OFDM, and PD-NOMA under low-SNR channels is analyzed and compared. Throughout the experiment, the channel of UE₁ was fixed with good channel quality, whereas the channel of UE₂ was set such that $|\mathbf{H}_{UE1}|^2 \simeq |\mathbf{H}_{UE2}|^2 + 6$ dB. The pattern matrix and user-stream allocation that were implemented are shown in Fig. 10. The modulation order applied is the highest order that the corresponding access scheme can support such that BER is below the FEC threshold. 4×4 and 4×8 matrices are implemented for OFDM and PD-NOMA, respectively, as two special cases of pattern matrices.

The BER of OFDM, PD-NOMA-SIC, and PDMA-MPA is shown in Fig. 10(a), (b), and (c), respectively. For OFDM, UE₁ with good SNR can transmit 64QAM, whereas UE₂ under channel degradation barely supports QPSK. The modulation spectral efficiency of OFDM is therefore $(6 \times 2 + 2 \times 2)/4 =$

 $4\ bits/symbol$. For PD-NOMA with SIC, UE $_1$ and UE $_2$ share the same REs using QPSK, the signal strength of UE $_2$ is around 6 dB less than UE $_1$ at the receiver. The average modulation spectral efficiency of PD-NOMA with SIC is: $(2\times 4+2\times 4)/4=4\ bits/symbol$, which is the same as OFDM in this case but with improved average BER of UE $_2$. In PDMA with MPA, 16QAM can be implemented for UE $_1$ due to the enhanced decoding accuracy. The average modulation spectral efficiency is $(2\times 2+4\times 4)/4=5\ bits/symbol$, outperforming both OFDM and PD-NOMA. Fig. 10(d) summarizes the experimental results of all three access schemes. It can be seen that PDMA can achieve higher modulation spectral efficiency with better BER performance compared to PD-NOMA-SIC when provided with ROP $> -3\ dBm$, validating the potential to support dynamic mmWave links in future-proof RANs.

V. CONCLUSION

The integration of PDMA with MPA has been proposed and applied to mmWave radio access systems using RoF mobile fronthaul. Through the selection and implementation of the pattern matrix, user-stream allocation, and stream amplitude/phase tuning, PDMA can provide improved access flexibility to cope with dynamic channel conditions of mmWave links. Moreover, PDMA stands out among conventional NOMA schemes with enhanced decoding accuracy provided by MPA. Using modified MPA process with improved convergence efficiency, our experimental demonstration of PDMA attained a 4 dB sensitivity improvement and proved the capability of recovering ambiguous symbols, in comparison with PD-NOMA-SIC. It is verified that PDMA can provide configuration flexibility, by evaluating the performance of PDMA with different pattern matrices and channel qualities. Furthermore, the ability of PDMA to support grant-free uplinks has been experimentally demonstrated to provide reduced BER penalty at the receiver compared to PD-NOMA-SIC. It is also verified that PDMA is capable of providing higher modulation spectral efficiency when part of the users in the system are limited by low-SNR channel qualities. In conclusion, PDMA integrated with MPA has been

systematically demonstrated and it has shown the potential to support future-proof mmWave-based radio access networks.

REFERENCES

- F. Lu, M. Xu, L. Cheng, J. Wang, and G.-K. Chang, "Power-division non-orthogonal multiple access (NOMA) in flexible optical access with synchronized downlink/asynchronous uplink," *J. Lightw. Technol.*, vol. 35, pp. 4145–4152, 2017.
- [2] Y. Alfadhli, M. Xu, S. Liu, F. Lu, P.-C. Peng, and G.-K. Chang, "Real-time demonstration of adaptive functional split in 5G flexible mobile fronthaul networks," in *Proc. Opt. Fiber Commun. Conf. and Exposition (OFC)*, San Diego, CA, USA, 2018, pp. 1–3.
- [3] Y. Saito, Y. Kishiyama, A. Benjebbour, T. Nakamura, A. Li and K. Higuchi, "Non-orthogonal multiple access (NOMA) for cellular future radio access," *Proc. IEEE 77th Veh. Technol. Conf. (VTC Spring)*, 2013, pp. 1–5.
- [4] LG Electronics, "Initial LLS evaluation for NCMA," 3rd Generation Partnership Project (3GPP), Tech. Rep. R1-1804576, Apr. 2018.
- [5] S. Chen, B. Ren, Q. Gao, S. Kang, S. Sun and K. Niu, "Pattern division multiple access A novel nonorthogonal multiple access for fifth-generation radio networks," in *Proc. IEEE Trans. Veh. Technol.*, vol. 66, no. 4, pp. 3185–3196, Apr. 2017.
- [6] L. Liu, E. G. Larsson, W. Yu, P. Popovski, C. Stefanovic, and E. de Carvalho, "Sparse signal processing for grant-free massive connectivity: A future paradigm for random access protocols in the internet of things," *IEEE Signal Process. Mag.*, vol. 35, no. 5, pp. 88–99, Sep. 2018.
- [7] Q. Zhou, S. Yao, S. Shen, Y. Chen, J. He, and G. Chang, "Efficient power-division NOMA for intelligent optical access network enabled by deep learning," *Proc. IEEE Photon. Soc. Summer Topical Meeting Ser. (SUM)*, 2019, pp. 1–2.
- [8] S. Shen, Y. Chen, Q. Zhou, and G. Chang, "Demonstration of pattern division multiple access with message passing algorithm in MMW-RoF systems," in *Proc. Opt. Fiber Commun. Conf. Exhibition (OFC)*, San Diego, CA, USA, 2020, pp. 1–3.
- [9] X. Dai, Z. Zhang, B. Bai, S. Chen, and S. Sun, "Pattern division multiple access: A new multiple access technology for 5G," in *Proc. IEEE Wireless Commun.*, vol. 25, no. 2, pp. 54–60, Apr. 2018.
- [10] Y. Alfadhli et al., "Latency performance analysis of low layers function split for URLLC applications in 5G networks," Comput. Netw., vol. 162, 2019. Art. no. 106865.
- [11] C. Wei, H. Liu, Z. Zhang, J. Dang, and L. Wu, "Approximate message passing-based joint user activity and data detection for NOMA," *IEEE Commun. Lett.*, vol. 21, no. 3, pp. 640–643, Mar. 2017.
- [12] B. Wang, L. Dai, Y. Zhang, T. Mir, and J. Li, "Dynamic compressive sensing-based multi-user detection for uplink grant-free NOMA," *IEEE Commun. Lett.*, vol. 20, no. 11, pp. 2320–2323, Nov. 2016.
- [13] R. Hoshyar, F. P. Wathan and R. Tafazolli, "Novel low-density signature for synchronous CDMA systems over AWGN channel," *IEEE Trans. Signal Process.*, vol. 56, no. 4, pp. 1616–1626, Apr. 2008.